REPORT DOCUMENTATION PAGE

Form Approved
OMB No. 0704-0188

1. REPORT DATE *(DD-MM-YYYY)*	**2. REPORT TYPE**	**3. DATES COVERED** *(From - To)*
June 2014	Technical Paper	June 2014- July 2014

4. TITLE AND SUBTITLE

Effect of Swirl on an Unstable Single-Element Gas-Gas Rocket Engine

5a. CONTRACT NUMBER
N/A

5b. GRANT NUMBER

5c. PROGRAM ELEMENT NUMBER

6. AUTHOR(S)

Harvazinski, M., Sankaran, V. and Talley, D.

5d. PROJECT NUMBER

5e. TASK NUMBER

5f. WORK UNIT NUMBER
Q12J

7. PERFORMING ORGANIZATION NAME(S) AND ADDRESS(ES)

Air Force Research Laboratory (AFMC)
AFRL/RQR
5 Pollux Drive
Edwards AFB CA 93524-7048

8. PERFORMING ORGANIZATION REPORT NO.

9. SPONSORING / MONITORING AGENCY NAME(S) AND ADDRESS(ES)
Air Force Research Laboratory (AFMC)
AFRL/RQR
5 Pollux Drive
Edwards AFB CA 93524-7048

10. SPONSOR/MONITOR'S ACRONYM(S)

11. SPONSOR/MONITOR'S REPORT NUMBER(S)
AFRL-RQ-ED-TP-2014-178

12. DISTRIBUTION / AVAILABILITY STATEMENT
Distribution A: Approved for Public Release; Distribution Unlimited

13. SUPPLEMENTARY NOTES
Technical paper presented at 50th AIAA/ASME/SAE/ASEE Joint Propulsion Conference, Cleveland, OH, 28-30 July, 2014.
PA#14333

14. ABSTRACT

In this study a series of three-dimensional unsteady reacting flow simulations are used to investigate the effect of swirl on the instability amplitude of a single-element gas-gas rocket combustor. The baseline combustor of interest is unstable because of a fuel cut-off event caused by the high-pressure waves in the combustor. Previous two-dimensional simulations have shown that swirl reduces the amplitude of the pressure oscillations compared with that of the baseline configuration. The current three-dimensional simulations show that swirl is indeed able reduce the amplitude of the instabilities, albeit not to the same extent observed in the two-dimensional simulations. We further observe that the enhanced mixing due to the swirling flow leads to a reduction in the recovery time associated with the fuel cut-off event, thereby allowing the combustor to experience a more continuous heat release. Nevertheless, unlike the two-dimensional case, the three-dimensional simulations show that the flame does not stay anchored to the dump-plane, which explains the higher relative amplitudes in this case.

15. SUBJECT TERMS

16. SECURITY CLASSIFICATION OF:			**17. LIMITATION OF ABSTRACT**	**18. NUMBER OF PAGES**	**19a. NAME OF RESPONSIBLE PERSON**
					V. Sankaran
a. REPORT	**b. ABSTRACT**	**c. THIS PAGE**	SAR	17	**19b. TELEPHONE NO** *(include area code)*
Unclassified	**Unclassified**	**Unclassified**			661-275-5534

Standard Form 298 (Rev. 8-98)
Prescribed by ANSI Std. 239.18

Effect of Swirl on an Unstable Single-Element Gas-gas Rocket Engine

Matthew E. Harvazinski*, Venkateswaran Sankaran†, and Douglas G. Talley‡
Air Force Research Laboratory, Edwards AFB, CA, 93524

In this study a series of three-dimensional unsteady reacting flow simulations are used to investigate the effect of swirl on the instability amplitude of a single-element gas-gas rocket combustor. The baseline combustor of interest is unstable because of a fuel cut-off event caused by the high-pressure waves in the combustor. Previous two-dimensional simulations have shown that swirl reduces the amplitude of the pressure oscillations compared with that of the baseline configuration. The current three-dimensional simulations show that swirl is indeed able reduce the amplitude of the instabilities, albeit not to the same extent observed in the two-dimensional simulations. We further observe that the enhanced mixing due to the swirling flow leads to a reduction in the recovery time associated with the fuel cut-off event, thereby allowing the combustor to experience a more continuous heat release. Nevertheless, unlike the two-dimensional case, the three-dimensional simulations show that the flame does not stay anchored to the dump-plane, which explains the higher relative amplitudes in this case.

I. Introduction

THE interaction between acoustics and combustion heat release can result in combustion instabilities. Lord Rayleigh in 1878 theorized that a positive feedback path can be established between the combustion heat release and acoustic pressure fluctuations leading to a progressive growth in the amplitudes.[1] While instabilities can be present in any combustion device, rocket engines are particularly susceptible because of their acoustically compact geometries. Consequently, the elimination and mitigation of combustion instabilities have been a part of nearly every major engine development project since the F-1 engine in the 1950s.[2,3] Despite several decades of active research, there is a lack of analytical models that are capable of predicting instabilities or understanding how they scale with size. This has given rise to the need for large numbers of full-scale tests and trial-and-error design changes, which are expensive and unpredictable. Today, combustion instability remains a major risk in the design and development of new liquid rocket engines. Recently, reacting flow computational fluid dynamics (CFD) simulations are starting to be successful in modeling combustion instability in a variety of configurations including gas turbines and rocket engines.[4–13]

The single-element engine chosen for this study is the continuously variable resonance combustor (CVRC) experiment. The CVRC is a gas-gas shear-coax rocket engine configuration that can be tuned to exhibit both stable and unstable combustion regimes. By changing the length of the oxidizer post, the amplitude of the pressure fluctuations and the frequency can be made to vary. Moderately stable combustion is observed at short lengths (9 cm) of the oxidizer post and stable combustion is observed for long lengths (19 cm). Between these limits, for intermediate post lengths, highly unstable combustion is present.[14] Pressure amplitudes at the unstable lengths can be in excess of 0.6 MPa (40% of the chamber pressure). High-fidelity CFD simulations of the CVRC geometry have been performed by using a variety of models and codes, a review of which is available in Ref. 4. The majority of the published results have focused on the unstable intermediate post-length cases and, in general, three-dimensional simulations have reproduced amplitudes slightly lower than those observed in the experiment. Direct comparisons between two and three-dimensional simulations

*Scientist, ERC Inc., AIAA Member.
†Senior Scientist, AIAA Member.
‡Research Physical Scientist, AIAA Associate Fellow.

have reported amplitude differences of about a factor of three, with the two-dimensional simulations having a lower amplitude.[6,7]

The CVRC computational studies have also revealed the underlying mechanisms that lead to the occurrence of instabilities. It is observed that when high-pressure waves in the head-end of the combustor enter the oxidizer post, there is a fuel cut-off event, which interrupts the combustion and locally extinguishes the flame. Once the wave has passed the fuel ports, the fuel supply is restored, but the lack of strong mixing leads to relatively weak combustion. It is only when the high pressure wave in the post returns after reflection that strong mixing takes place due to baroclinic vorticity generation and significant combustion heat release resumes. This cycle of flame unsteadiness operates in close synchronization with the pressure dynamics in the main combustor leading to a continual growth of the pressure oscillations and the onset of a limit cycle. On the other hand, under stable operation, the fuel cut-off event is either absent or weak and there is a more or less continuous presence of combustion heat release, which prevents the pressure cycle from building up. We can thus see that the combustion stability dynamics are strongly controlled by the flame dynamics and the heat release process.

To date, swirl has not been added to the CVRC experiment, although it has been recently studied computationally in two-dimensional simulations.[15] The interest in the effect of swirl arises because it has been widely used as a stabilization mechanism for a variety of combustion systems including gas turbines, rocket engines, and industrial furnaces. Swirl can have dramatic effects on the flowfield; these include jet growth, entrainment, flames size and shape, combustion intensity, and instability.[16] In gas turbine applications the geometry and swirl allows for the formation of a central toroidal recirculation zone (CTRZ) which is associated with high shear stress and vortex breakdown.[17] The CTRZ forms when the swirl number is above a critical value, typically 0.6, under which conditions, an adverse pressure gradient forms causing flow reversal in the central region of the jet.[16] In rocket engines, swirl injectors have several advantages over jet-type injectors; they are less sensitive to manufacturing defects and are less susceptible to cavitation. Some high frequency instabilities have also been suppressed using swirl type injectors.[18] Despite these advantages, the presence of swirl does not guarantee stable combustion. Martin et al. simulated a premixed swirl injector, which showed self-excited instability when the outlet boundary condition was acoustically closed despite the presence of swirl.[13] The afore-mentioned two-dimensional simulations indicated that that adding swirl is indeed stabilizing for the CVRC configuration. In the present work, we extend these swirl studies to more realistic three-dimensional situations and examine the underlying physical mechanisms that influence the occurrence of combustion instabilities.

Four simulations are considered in the present research study, namely, a baseline simulation without swirl and three simulations with different strengths of swirling flow. All four simulations focus on the unstable regime of the CVRC operations. The baseline simulation is the same as what was used previously to compare with experimental data[4,19] and corresponds to the case of maximum instability amplitude. The remainder of the paper is organized as follows. First, additional background information related to the CVRC computations and parametric behavior are given. Details of the simulation including the implementation of the swirling flow are given in the next section. Following this, we present the results of the comparison between the baseline and the three swirl simulations. A summary of the findings is given in the final section.

II. Instability Mechanisms

Recent work has shed light on the instability mechanisms in the CVRC configuration. Here, a brief summary of the relevant aspects is given while complete details can be found in Harvazinski et al.[4] The key source of the instability arises due to a fuel cut-off event. The first image in Figure 1 illustrates this event at the point when the head end of the combustor reaches the high pressure point in the acoustic cycle in the combustor. The pressure wave at the head end of the combustor reflects downstream into the combustor and also propagates upstream into the oxidizer post. When the wave in the oxidizer post passes over the fuel injection region in the post, it disrupts the fuel flow. In fact, the figure shows that the fuel is completely absent from the near-wall region, which is a result of the fuel being pushed back by the high pressure. Local pockets of combustion in the cup are visible which consume any lingering fuel. The local combustion is a result of increased mixing due to the elevated baroclinic torque caused by the high-amplitude pressure wave. In the immediate aftermath of the fuel cut-off event, combustion heat release in the combustor moves downstream of the dump plane. This movement allows the incoming fuel to enter the combustor without burning immediately, a consequence of the slow mixing in the diffusion layer between the fuel and oxidizer.

Consequently, a significant amount of fuel accumulates in the head end of the combustor before reignition takes place.

The second image in Figure 1 shows the reignition event. When the pressure wave in the oxidizer post returns to the combustor, it expands around the back step corner. As it expands, it forces the unburnt fuel into the recirculating gases causing combustion to take place near the backstep. The large amount of fuel that has collected at the head-end now burns, leading to a rapid increase in the pressure. This rise in pressure is in synchronization with the acoustic wave in the combustor, which further amplifies the combustion and causes an even higher pressure rise. In turn, this sets up the fuel cut-off event for the next acoustic cycle. For lower levels of instability that occur for the stable configurations, the fuel cut-off is absent and there is a more continuous heat release throughout the cycle. Thus, the elimination or reduction the effect of the fuel cut-off event seems to have the potential to lower the amplitude of the instability.

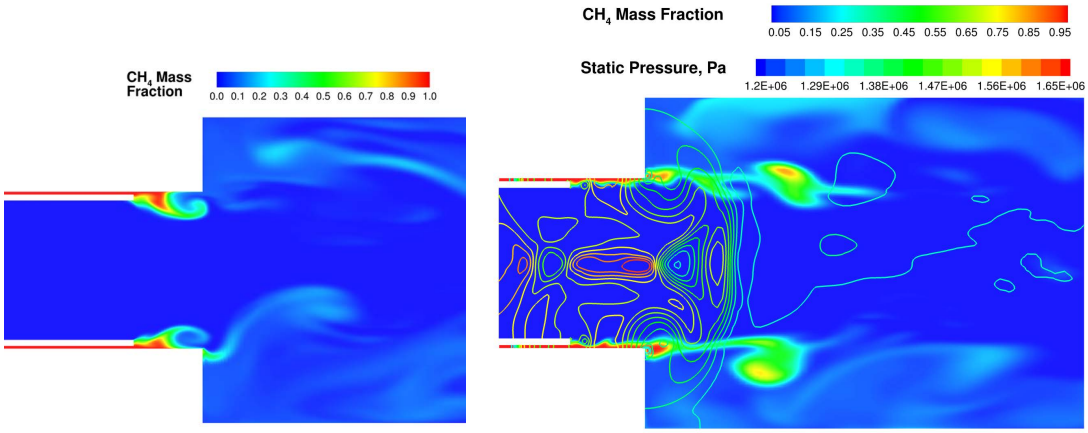

Figure 1: The fuel cut-off event is shown on the left. The slice near the backstep shows the disrupted fuel flow into the combustor after the high-pressure wave moved through the oxidizer post. The image on the right shows the post-coupled reignition event. Lines are colored with static pressure.

In an attempt to control the level of instability, a number of design changes were considered using two-dimensional simulations.[15] Of these options, the inclusion of swirl proved to be very successful. Several levels of swirl were tested and the results showed that the resulting pressure amplitudes were reduced by as much as 55-70%. In fact, for the higher-swirl cases the flame remains attached to the dump plane throughout the acoustic cycle. Close examination of the results reveal that the radial pressure gradient, which is proportional to the swirl velocity, allows a thin film of methane to remain along the wall even when the rest of the fuel flow is cut-off. In turn, this provides a constant source of fuel to the flame, reduces the flame unsteadiness and leads to lower levels of pressure oscillations.[4]

While the two-dimensional simulations are promising, there is some reason to be cautious about drawing definitive conclusions. For instance, previous studies have shown that two-dimensional simulations are effective in capturing qualitative trends, but some key quantitative deficiencies are also evident. First, the pressure amplitudes in the two-dimensional simulations are about three times lower than the three-dimensional results and experiments. In addition, the two-dimensional simulations also do a poor job in resolving the higher order harmonics that are typically seen in longitudinal instabilities. Moreover, in the upstream region of the oxidizer post, the flow is highly unsteady and strongly three-dimensional, which also influences the strength of the vortices in the post and combustor. For these reasons, it is extremely important to employ detailed three-dimensional simulations and obtain an accurate representation of the effects of swirl. Moreover, the three-dimensional solutions will also yield a better description of the swirl flowfield and its coupling with the combustion and acoustics phenomena.

III. Simulation Details

The three-dimensional simulations in the present study are run using GEMS, a second-order finite volume based CFD code that solves the coupled continuity, momentum, energy, turbulence, and species equations. An implicit dual time scheme, which allows for high aspect ratio grids at the wall, is used.[20–22] Combustion is modeled using a single step global reaction for methane[23] with laminar kinetics, allowing the coupling between the chamber acoustics and heat release to be captured. Turbulence is modeled using a hybrid RANS/LES approach,[24,25] with the two-equation k-ω turbulence model used for the near wall and under resolved regions.[26]

Three swirl angles are considered, 3° 9° and 15°. This corresponds to swirl numbers between 0.03 and 0.18, where the swirl number is defined as the ratio of angular and axial momentum. For the baseline case, the swirl number and angle are zero. For swirl numbers less than 0.4, the flow is characterized having weak swirl.[16] Swirl is typically introduced through vanes, which turn the incoming fuel through a specified angle. Such an approach would mean that each case would require a separate mesh. To reduce the amount of grid generation, the swirling fuel flow is introduced at the inlet boundary by specifying a swirl angle. The swirl velocity is related to the axial velocity through the equation,

$$u_\theta(r) = u \cdot \left(\frac{r}{R_s}\right) \sin(\theta_S) \tag{1}$$

Where r is the radius, R_S is the radius of the injector, and θ_S is the swirl angle.

Operating conditions for the simulations are shown in Table 1; the only change to the operating conditions for each of the four cases is the swirl angle. A schematic of the computational domain is shown in Figure 2. Decomposed hydrogen peroxide is used as the oxidizer; it enters the domain upstream of a series of choked slots. The oxidizer post length is fixed at 13.97 cm for this study. Fuel, gaseous methane, is injected upstream of the dump plane. The combustor has a fixed length of 38.1 cm and a choked converging-diverging nozzle is affixed to the downstream end of the combustor. The choked slots and nozzle provide acoustically closed boundary conditions, allowing the majority of the oxidizer manifold to be neglected from the model. All computations utilize an adiabatic wall boundary condition. A hexahedral mesh with 5 million cells is used for the computation. An estimate of the grid resolution required was performed using a combination of two- and three-dimensional simulations and can be found in Ref. 7.

Table 1: Operating conditions for the CVRC.

Parameter	Value
Fuel mass flow rate, kg/s	0.027
Fuel temperature, K	300
Oxidizer mass flow rate, kg/s	0.320
Oxidizer temperature, K	1030
Oxidizer percent H_2O	57.6
Oxidizer percent O_2	42.4
Equivalence ratio	0.80
Swirl angle, deg	0 – 15

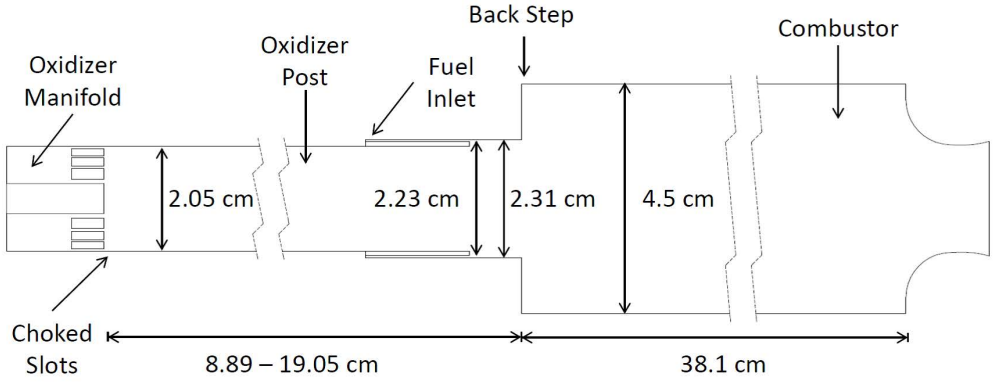

Figure 2: Schematic of the CVRC computational domain. For the present configuration, the oxidizer post length is fixed at 13.97 cm.

The flowfield is initialized with quiescent conditions at a uniform pressure of 1.4 MPa. The oxidizer post is filled with oxidizer at 1030 K, the fuel injection annulus is filled with methane at 300 K, and the combustor is filled with a mixture of water and carbon dioxide at 1500 K. The warmer temperature in the combustor enables the auto ignition of methane. At the start of the simulation, diaphragms at the inlets and outlet are broken and a flowfield is quickly established. Ignition takes place approximately 2 ms from the start of the simulation. The simulations are run with a time step of 0.1 μs for a duration of 40 ms. The relatively short initial transient ($<$ 5 ms) and long run-time provide sufficient cycles for analysis.

IV. Results

A. Power Spectral Density Analysis

The raw pressure signals for the baseline and two of the swirl cases are shown in Figure 3. The 15° case is omitted for clarity but has a similar amplitude to the 9° case. The measurement location is 1.27 cm from the backstep on the wall. The signals show that the amplitudes of the two swirl cases are noticeably smaller than that of the baseline case. The overall peak-to-peak amplitude of the baseline non-swirl case is approximately 650 kPa, while the three swirl cases all have similar amplitudes, approximately 425 kPa. The lower amplitude results in a waveform that is less steepened. The trough of the waves for the swirl cases is also observed to be broader and shows evidence of additional unsteadiness compared to the non-swirl result. This unsteadiness appears to be related to the timing of the heat release, which is described in the subsequent sections.

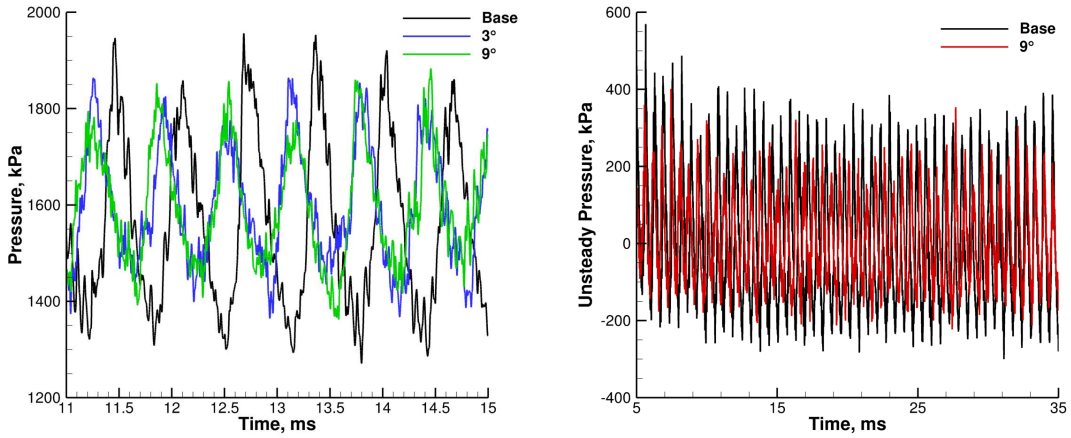

Figure 3: The left image is the raw pressure signal shown for a 4 ms window. The case with 15° of swirl is omitted for clarity but has a similar amplitude as the 9° case. The image on the right is a 30 ms snapshot of the baseline and 9° case and shows the pressure fluctuation.

A quantitative interrogation of the pressure data can be performed using a power spectral density (PSD) analysis. Computational data are sampled at a rate of 10 MHz and a total of 35 ms of data are used for analysis. This provides a frequency resolution of 28.5 Hz and a maximum frequency of 5 MHz, well above the level of interest for longitudinal modes. PSD plots for the four cases are shown in Figure 4. Several differences between the baseline and swirl cases are apparent. First is the lack of organized higher-order harmonics for the swirl cases. The baseline case shows well-defined harmonics up to 10 kHz, while all three swirl cases show less resolved higher-order modes above 5 kHz. It should be noted that experimental PSDs without swirl (not shown) resemble the baseline case with clearly recognizable higher order modes.[4]

The PSD data can be further interrogated by integrating the area under the peaks. This provides the peak-to-peak amplitude associated with each mode. The integration is performed using the full-width half-max method, which is a more quantitative method to compare the amplitudes of each mode as opposed to the height of the peaks on the PSD.[27] A summary of the amplitudes and frequencies is shown in Table 2:.

The frequency is altered slightly between the swirl and non-swirl cases, with the 3° case showing the largest shift. The slightly higher frequency agrees with the elongated wave trough that was seen in Figure

3. Overall, the modal amplitudes are lower with swirl. The amplitude of the first mode in the 9 swirl case shows the greatest reduction–a reduction of 29%–compared to the 3° case, where the amplitude is reduced by 24%. Interestingly, in the two-dimensional study, 9° swirl case also showed the greatest amplitude reduction with somewhat diminishing returns for higher levels of swirl.[15] For the 9° case, the reduction in the second and third modes is approximately 30%, while a slightly lower reduction is predicted for the 3° and 15° cases. Overall, we note that the amplitude reduction is less compared to the prior two-dimensional study (which was as high as 70%).

All three configurations with swirl show a new excited mode between the first and second modes, albeit with a lower amplitude. This is not visible in the baseline and is not seen in the experimental configuration. The exact nature of this mode is not known. The pressure signals shown in Figure 3 are recorded at four different circumferential locations and the signals from each show no apparent phase shift between the locations, indicating that this is not a traveling or oscillating transverse mode. Similarly, visualization of the three-dimensional flowfield over multiple cycles shows no apparent precessing vortex core (PVC) mode that is often associated with swirling flows.[16,17] Previous results for a shorter 9 cm oxidizer post length without swirl also showed a similar unidentified mode between the first and second modes around 2800 Hz,[4] although corresponding experimental results at this length did not show evidence of this mode.

Table 2: Frequency and integrated peak-to-peak pressure amplitudes.

Mode	Baseline		3°		9°		15°	
	f, Hz	p', kPa	f, Hz	p', kPa	f, Hz	p', kPa	f, Hz	p', kPa
1	1543	349.10	1600	265.88	1571	248.80	1571	251.77
Unknown	–	–	2886	17.37	2714	29.72	2714	21.55
2	3114	87.55	3171	61.19	3171	60.66	3171	66.19
3	4629	36.25	4723	28.47	4723	25.59	4723	27.65

B. Cycle Description

This section presents an overview of a single cycle for the baseline case contrasted with the 9° swirl case. The 3° and 15° cases behave similarly to the 9° case and are not presented. A complete description of the baseline cycle can be found in Ref. 4 and the focus here is on the comparison to elucidate the effects of swirl on the instability mechanisms. The pressure time history for each case is shown in Figure 5. The cycle for each case is representative of the overall behavior of the simulation. For both cases, the start point of the cycle is when the head end of the combustor is at the maximum pressure.

Figure 6 and Figure 7 show the time evolution of a single cycle for each of the six points marked in Figure 5. Figure 6 shows the heat release contours along with an isoline of 2000 K and an isoline for the stoichiometric mixture fraction. Figure 7 shows the fuel (methane) mass fraction contour along with static pressure lines. At the beginning of the cycle there is significant heat release taking place in both cases with a flame attached to the back step corner. The setup of the fuel cut-off event is evident in both cases where the high-pressure wave has just moved passed the injection point and the incoming fuel has been displaced. At the second time instance, the pressure in the head end of the combustor has decreased. The fuel cut-off has caused the flame to detach and move downstream while unburned fuel starts to fill the combustor behind the burning. This is different from the two-dimensional swirl results discussed earlier, which showed that the swirling flow enables the flame to remain attached throughout the cycle.[15]

Beyond this point in the cycle, the two cases follow different paths. At time 3, the pressure has reached a minimum. In the no-swirl case, the flame continues to move further downstream and a large amount of fuel fills the combustor. Contrasting this with the swirl case, we see that fuel in the shear layer is already being consumed and there is combustion taking place in the vicinity of the backstep, but not at the corner. Moving from time 3 to 4 the non-swirl images look very similar. One difference, which is difficult to discern, is that there is now heat release at the backstep corner. This is caused by the returning wave pushing the accumulated fuel into the warm recirculating combustion products. (A picture of this event was shown in Figure 1.) At time 4, the swirl case shows heat release primarily taking place downstream along with a noticeable reduction in the amount of methane.

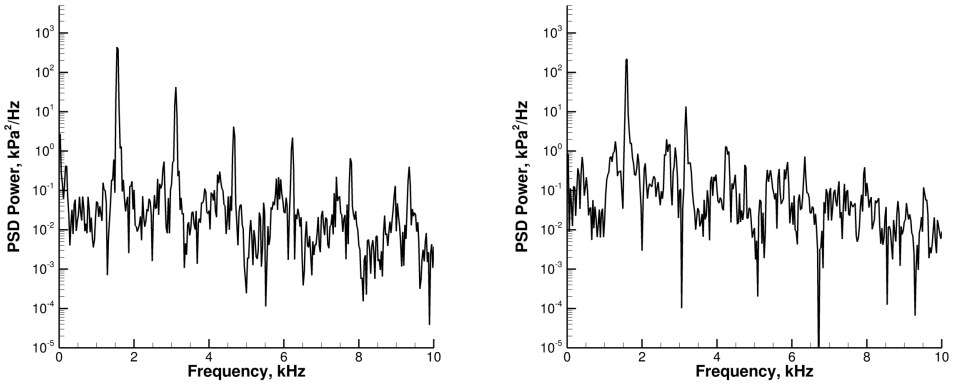

(a) Baseline.

(b) 3° of swirl.

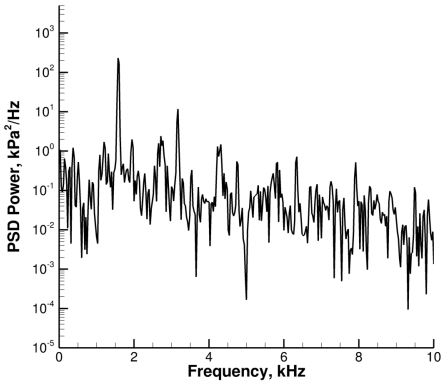

(c) 9° of swirl.

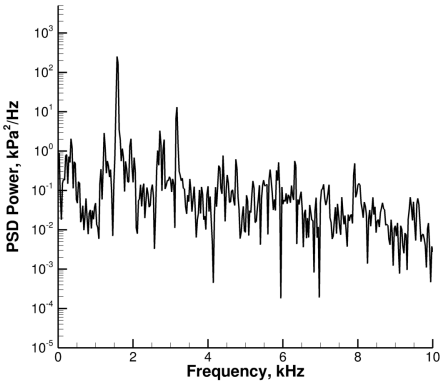

(d) 15° of swirl.

Figure 4: PSD plots for the four simulations, point of analysis is on the combustor wall 36.8 cm from the back step.

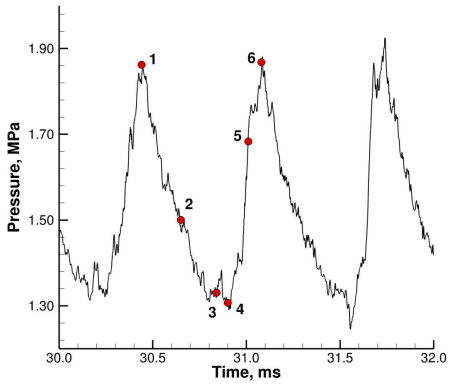

(a) Baseline.

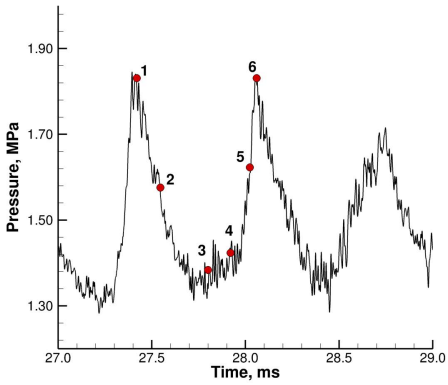

(b) 9° of swirl.

Figure 5: Points of analysis for the cycle description for the baseline and 9° swirl case. Points of analysis occur at approximately the same instants in the cycle.

At time 5, the pressure at the head-end is starting to increase and combustion is taking place in both cases. The flowfield regions which are combusting are however noticeably different. For the swirl case, the combustion is confined to the region around the shear layer. Without swirl, the large amount of methane, which has filled a portion the recirculation region, starts to burn and there is evidence of significant heat release near the wall. At time 6, the recirculation region in the swirl case continues to be free of heat release unlike the baseline case. There is also more unburned methane lingering in the recirculation region of the baseline case.

The key difference revealed by the cycle analysis lies in the timing of the start of combustion following the fuel cut-off event. For the baseline non-swirl case, combustion does not begin until the returning oxidizer post wave returns, occurring at the 60% mark in the cycle. With swirl, however, the combustion reinitiates sooner, well before the low-pressure point in the cycle. The faster reignition of combustion with swirl allows less unburned methane to accumulate in the combustor and provides a more continuous heat release throughout the cycle. The unsteadiness that was visible in the pressure signal (Figure 3) for the swirl case is a result of this continuous heat release, which provides additional pressure perturbations. Of course, the continuous heat release also results in the lower amplitudes of the pressure oscillations shown in Figures 3 and 4.

C. Time Averaged Flowfield

The differences in the cycle between the swirl and non-swirl configurations results in noticeably different time averaged heat release distributions as evident in Figure 8, which shows an axial slice of the time-averaged heat release along with several temperature isolines. The figure shows the baseline and the 9° swirl cases. The flowfield for the other two swirl cases is similar to the 9° case with minor variations in the axial extent of the temperature isolines. With regard to the baseline and swirl cases, there are several noticeable differences. First, the baseline configuration shows a distinctive hump in the heat release contours that extends out from the shear layer into the recirculation region, indicating that there is more combustion occurring in the recirculation region for the baseline case. On the other hand, the heat release for the swirl case is primarily confined to the shear layer, with the peak heat release extending over a greater axial distance. The baseline also shows more heat release extending further upstream into the cup of the injector.

Isolines of the time-averaged temperature show that the axial extent of the core oxidizer flow, demarcated by the 1200 K line, is similar for both cases. The axial extent for the higher temperatures is, however, pushed further downstream. This indicates that the presence of swirl causes the combustion to take place over a larger axial distance. Recall that the cycle analysis showed that a significant portion of the combustion in the baseline occurred during the post-reignition event whereas with swirl, the heat release occurs more uniformly during the cycle, consuming the methane and oxidizer gradually. The time-averaged recirculation region (not shown) is similar for both the swirling and non-swirling cases indicating that the relatively small amount of swirl introduced through the fuel injector does not alter the global recirculation region.

It is also noteworthy that the present swirl results do not show the presence of a CRTZ region which may be attributed to the absence of a central hub and the relatively low swirl. Interestingly, the earlier two-dimensional simulations seemed to indicate the presence of a CTRZ, although this was not previously reported.[15] Figure 9 shows the associated streamlines for the two-dimensional simulation with a swirl angle of 9°; in the figure, the CTRZ is clearly evident. The presence of the CTRZ may help to keep the flame attached (as is the case in the 2D case). However, it is possible that the CTRZ formation is a result of the 2D symmetry along the axis, which creates an artificial "wall-like" effect that does not allow flow to penetrate. As mentioned above, the three-dimensional flowfield, which has no such restriction, does shows no evidence of the CTRZ.

D. Fuel Cut-Off Recovery

The key aspect of the combustion instability mechanism in the CVRC configuration is the fuel cut-off event. Following the cut-off event, the heat release moves downstream allowing the methane to fill the combustor without burning. Once this accumulated fuel burns a large pressure spike results because of the heat release and associated gas expansion. Between the baseline and swirl cases, we have already noted the differences in the timing and the location of this heat release. The accumulation of methane in the combustor is shown in Figure 10 for both cases. The figure shows an isosurface representing 25% methane at the midpoint of the cycle and three-quarters of the cycle. By the midpoint in the cycle, both results show that there is a significant amount of fuel accumulated in the combustor. With the addition of swirl, there is a gap in the

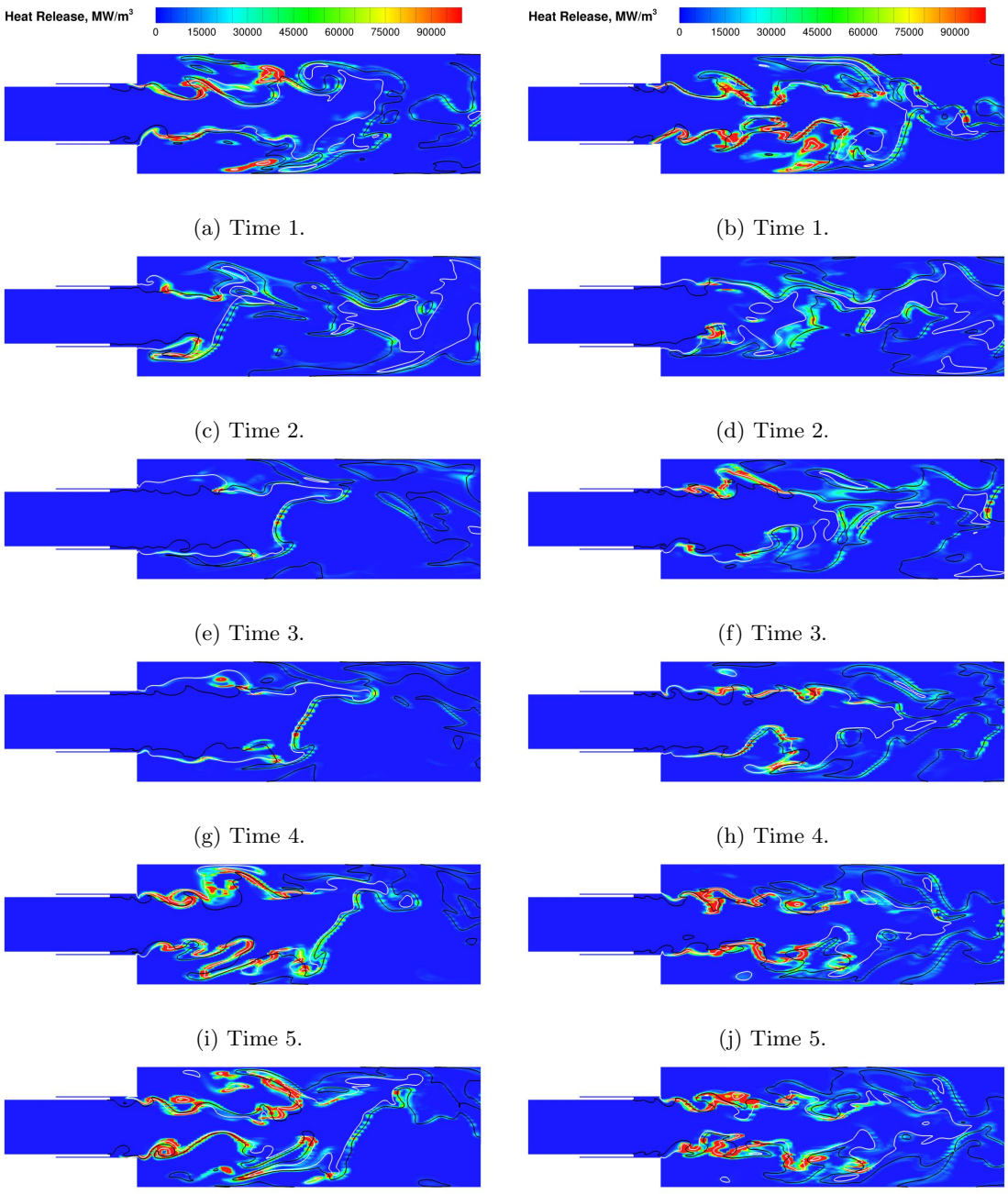

(a) Time 1.

(b) Time 1.

(c) Time 2.

(d) Time 2.

(e) Time 3.

(f) Time 3.

(g) Time 4.

(h) Time 4.

(i) Time 5.

(j) Time 5.

(k) Time 6.

(l) Time 6.

Figure 6: Time evolution of heat release contours for a single cycle. Right images show the baseline case without swirl and the images on the left show the case with 9° of swirl. Contours are heat release, the white line is an isoline of 2000 K and the black line is an isoline of the stoichiometric mixture fraction.

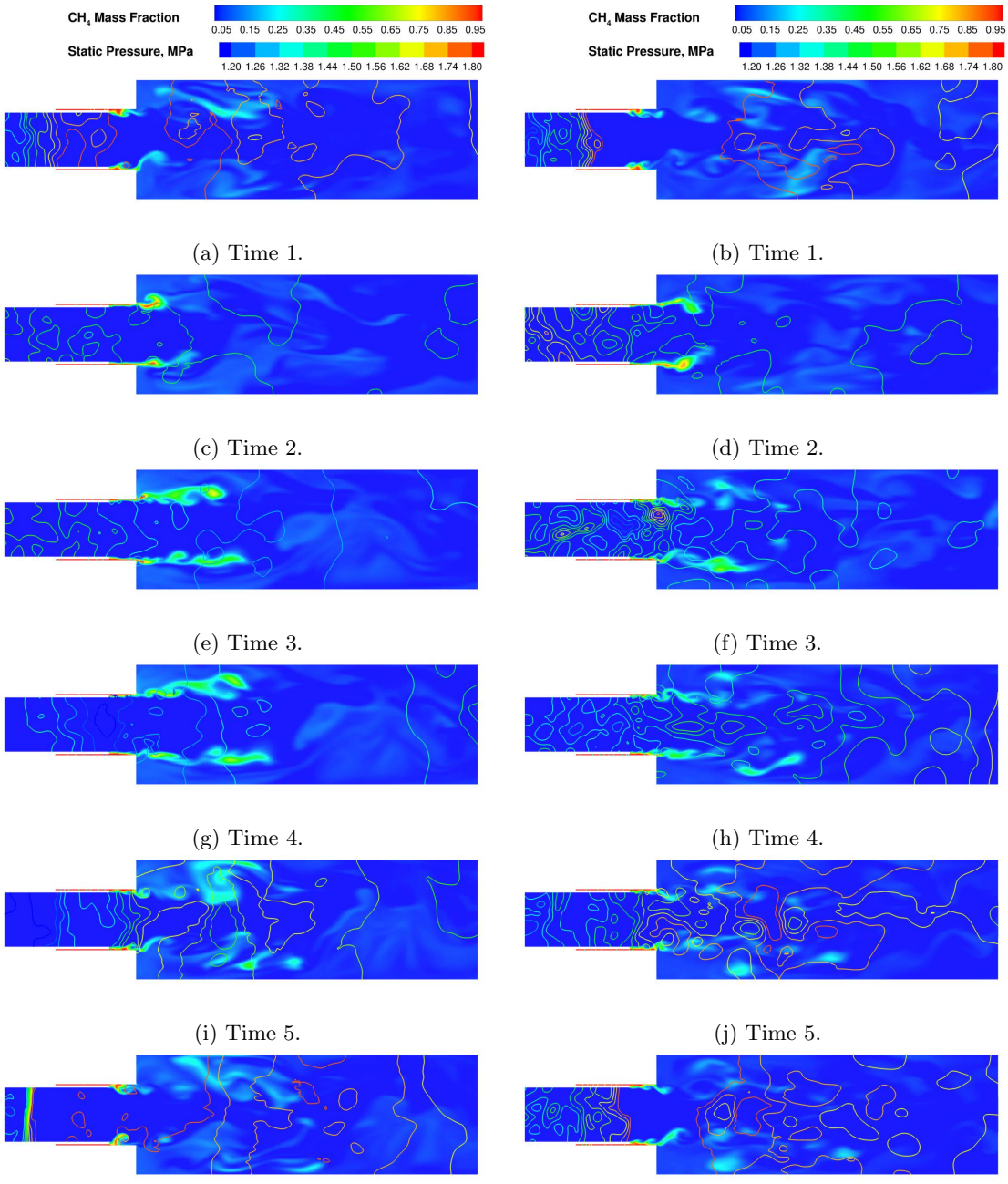

(a) Time 1.

(b) Time 1.

(c) Time 2.

(d) Time 2.

(e) Time 3.

(f) Time 3.

(g) Time 4.

(h) Time 4.

(i) Time 5.

(j) Time 5.

(k) Time 6.

(l) Time 6.

Figure 7: Time evolution of CH_4 mass fraction for a single cycle. Right images show the baseline case without swirl and the images on the left show the case with 9° of swirl. Contours are CH_4 mass fraction; lines are colored with static pressure.

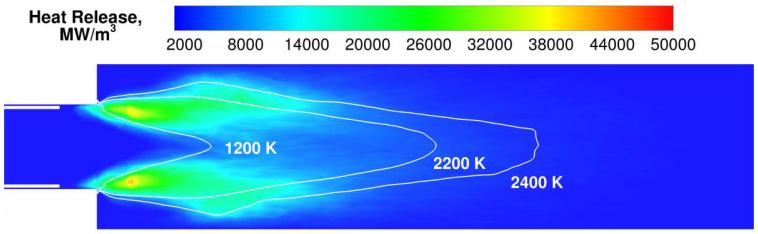

(a) Baseline.

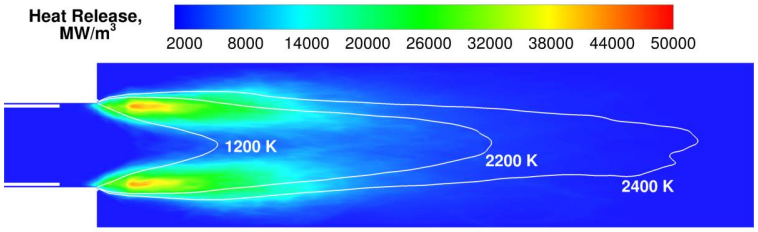

(b) 9° of swirl.

Figure 8: Time averaged heat release contours for the baseline and 9° swirl cases. Three time averaged temperature isolines for 1200 K, 2200 K, and 2400 K are plotted. Flowfield for remaining two swirl cases is similar with slight differences in the axial extent of the 2200 K and 2400 K temperatures lines.

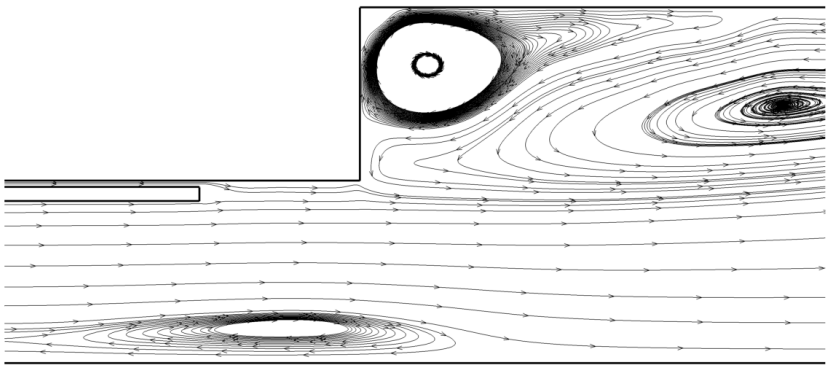

Figure 9: Time averaged streamlines for a two-dimensional simulation with a swirl angle of 9°. There is a CTRZ located along the axis just before the combustor.

methane just downstream of the combustor. It is near this point where heat release starts to take place. By the three-quarter mark, the swirl case shows notably less accumulated unburnt fuel in the combustor compared with the baseline case.

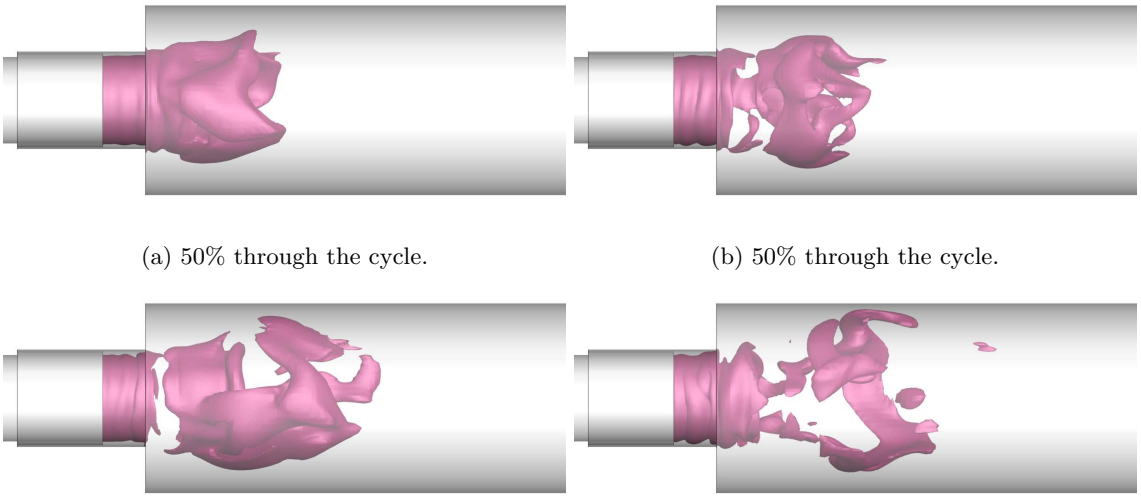

(a) 50% through the cycle.

(b) 50% through the cycle.

(c) 75% through the cycle.

(d) 75% through the cycle.

Figure 10: CH_4 mass fraction for the baseline (left) and 9° swirl (right) cases. The isosurface represents 25% methane and is shown at two points in the cycle: half way through and three-quarters of the way through.

The decreased accumulation of methane is the result of the more continuous heat release in the cycle for the swirl case. A series of temperature contours are shown in Figure 11. The slice is 1 cm downstream of the backstep and the dotted circle in the center represents the diameter of the oxidizer post. Near the beginning of the cycle, the swirl shows a smaller core region of oxidizer, largely inside the diameter of the oxidizer post with the recirculation region at a uniform temperature unlike the baseline, which shows a larger radial spreading of the oxidizer. In the baseline case, 40% of the way through the cycle there is significantly more unburnt fuel entering the combustor. This is indicated by blue regions, which indicate the lower fuel temperature compared to the warmer oxidizer. These blue regions are also visible in the swirl case but the region is smaller, and shows less radial extent away from the oxidizer post diameter. Overall, we can observe that the swirling flow increases the fuel-oxidizer mixing.

The differences between the flowfields are more obvious at 70% through the cycle. The baseline case shows a nearly uniform ring of unburnt fuel, with the ring being aligned with the oxidizer post diameter. The oxidizer has also spread radially outward past the diameter of the oxidizer post. The swirl case shows localized regions of fuel, but overall these regions are better mixed with the oxidizer as indicated by the higher overall temperature. The oxidizer also does not radially extend outward past the oxidizer post diameter. By the 80% point in the cycle, the flowfields return to a similar point where the fuel at the 1 cm location is nearly consumed just prior to the fuel cut-off event being set up. Overall, the swirl appears to promote better mixing which largely confines the incoming fuel to the shear layer near the backstep. The increased mixing allows combustion to take place sooner in the cycle; this limits the amount of unburnt fuel that can accumulate. By altering the timing of the combustion following the fuel cut-off event the swirling flow is therefore able to decouple somewhat the combustion heat release and the acoustics.

E. Mode-shape Analysis

Mode shapes for the pressure and heat release are constructed by volume averaging the pressure and heat release within thin axial disks. The averaged data in these disks is then filtered and phase-averaged to generate a mode-shape. Full details on the procedure can be found in.[28] Figure 12 shows the first longitudinal mode-shape for the baseline case and for the 9° swirl case. As expected the amplitude of the swirl case is lower. The mode-shape for the swirl and baseline have a similar shape in the combustor with a node in the center. The swirl mode-shape at the end of the combustor is smoother than that of the baseline case, possibly

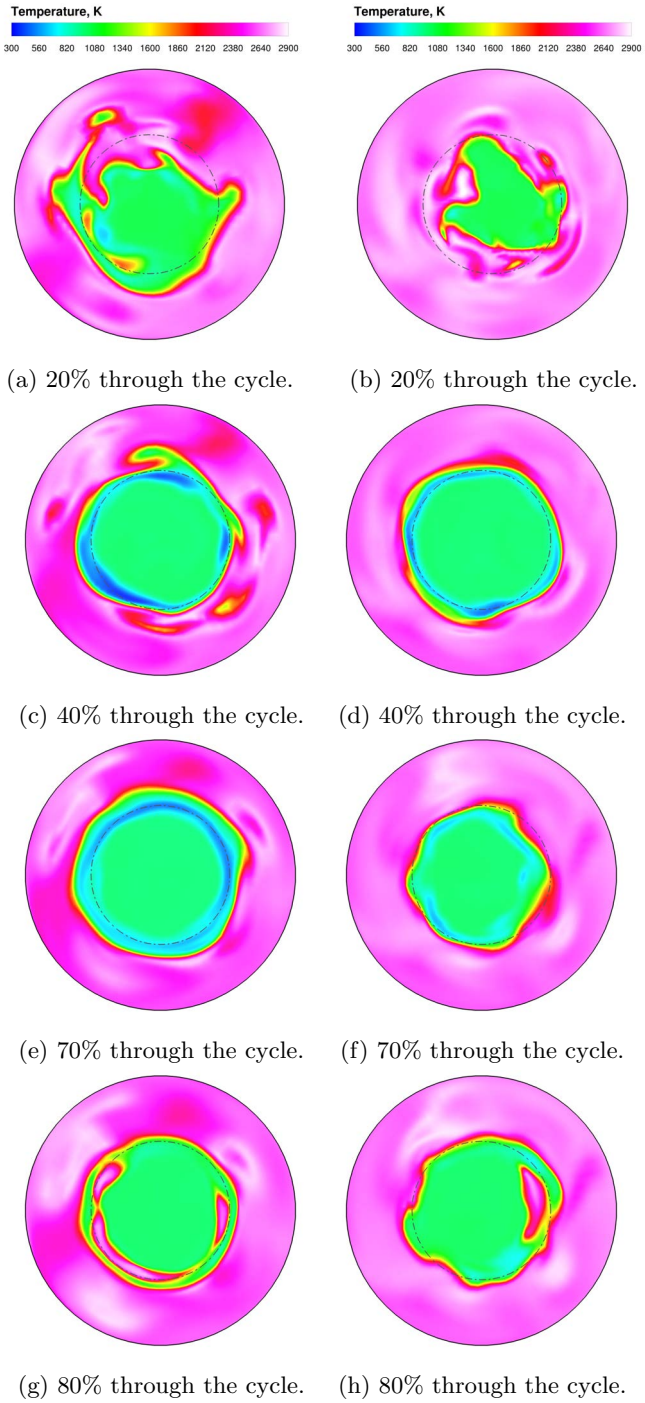

(a) 20% through the cycle. (b) 20% through the cycle.

(c) 40% through the cycle. (d) 40% through the cycle.

(e) 70% through the cycle. (f) 70% through the cycle.

(g) 80% through the cycle. (h) 80% through the cycle.

Figure 11: Temperature slices 10mm downstream from the dump plane. Dashed circle indicates the diameter of the oxidizer post. The baseline case is shown on the left and the 9° of swirl on the right. Notice in the baseline case as the cycle progresses there is a large expanse of oxidizer and fuel in the center, extending past the oxidizer post diameter. In the swirl case this occurs only up to 40% through the cycle, past that point there is burning in the shear layer which does not allow as much fuel to accumulate.

reinforcing the assumption that there is less coupling between the heat release and pressure. The mode-shape in the oxidizer post is also different showing less variation than the baseline case. Combustion heat release mode-shapes again show the difference in amplitude but are otherwise similar showing a characteristic double-peaked structure.

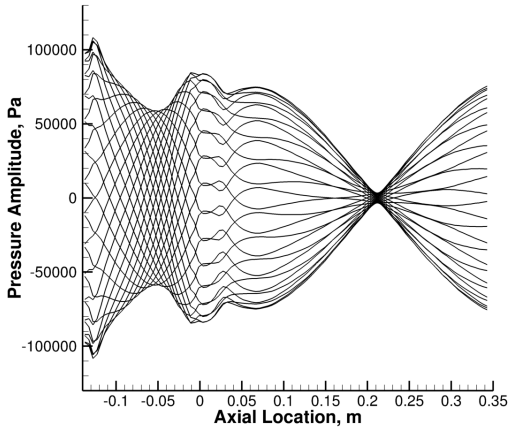

(a) Baseline, pressure.

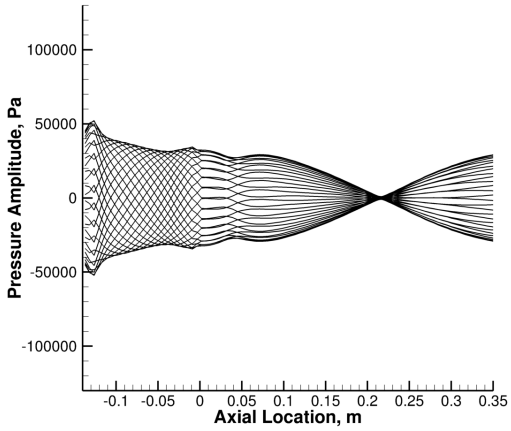

(b) 9° swirl, pressure.

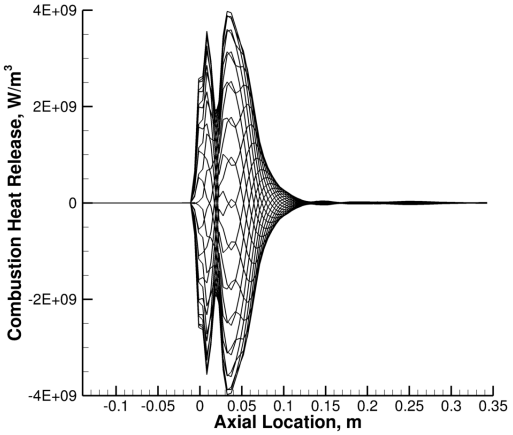

(c) Baseline, combustion heat release.

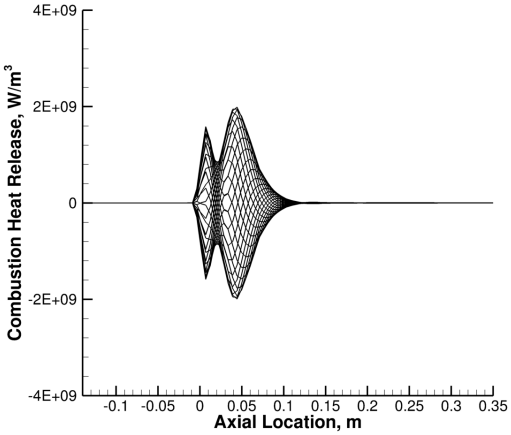

(d) 9° swirl, combustion heat release.

Figure 12: Mode-shapes for the first longitudinal mode.

The pressure mode-shapes for the unidentified mode between the first and seconds modes in the swirl cases are shown in Figure 13. The mode-shapes have a similar structure in the combustor and take the form of what appears to look like a second longitudinal mode. In the oxidizer post, each case shows slightly different behavior, which may indicate that this mode corresponds to some form of combined mode for the post-combustor configuration.

V. Conclusions

The effect of swirl has been investigated numerically for a single element rocket engine, which exhibits strong longitudinal combustion instabilities. Previous two-dimensional results showed that the addition of swirl could help mitigate the fuel cut-off event, which is responsible for driving the instability. Three-dimensional simulations show that the addition of swirl indeed lowers the instability amplitude but not to the same extent as was observed in two-dimensions. The addition of swirl was able to reduce the amplitude by

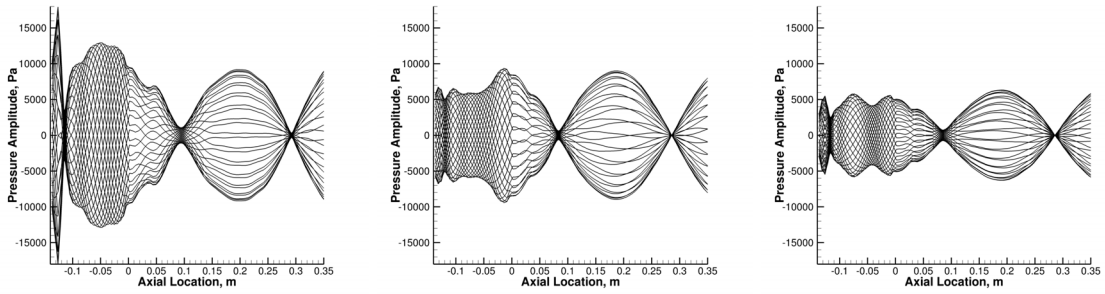

(a) 3° swirl, pressure. (b) 9° swirl, pressure. (c) 15° swirl, pressure.

Figure 13: Pressure mode-shapes for the unknown mode between the first and second modes.

approximately 30%. This is possibly because the two-dimensional simulations have lower overall instability amplitudes, which makes it easier for nominal amounts of swirl to suppress the fuel cut-off event. The three-dimensional baseline no-swirl case has higher amplitude pressure oscillations and the swirl levels used in this study are not strong enough to counter the pressure waves as effectively. Moreover, the two-dimensional simulation also showed the presence of a CTRZ, which is known to have a stabilizing effect; however, this structure is not evident in the three-dimensional simulations. We note that its presence in two-dimensions may well be a result of the artificial axis boundary condition. These results clearly point to the limitations of two-dimensional simulations for drawing quantitative conclusions and the resultant need for detailed three-dimensional simulations.

The three dimensional results indicate that swirl is effective in lowering the amplitude by of the pressure oscillations by about 30%, although this effect seems to level off with increasing amounts of swirl. The underlying mechanism is related to modifications in the behavior following the fuel cut-off event. The swirling flow enhances the mixing of the fuel and oxidizer, and the propellants begin to burn sooner after the fuel cut-off. This means that less unburned fuel accumulates in the combustor, which in turn has the effect of an even combustion heat release. The continuous heat release and the absence of a large combustion event (as in the case of the non-swirl case when the accumulated fuel finally burns) lead to a reduction in the coupling between the combustion heat release and acoustic pressure. However, we point out that the swirl effect is not strong enough to keep the flame attached (as in the two-dimensional case) and completely stabilize the combustion response.

Acknowledgments

Computing resources were provided by the DoD High Performance Computing Modernization Program.

References

[1]Rayleigh, J., "The Explanation of Certain Acoustical Phenomena," *Nature*, Vol. 18, 1878, pp. 319–321.

[2]Blomshield, F., "Historical Perspective of Combustion Instability in Motors: Case Studies," *37th AIAA/ASME/SAE/ASEE Joint Propulsion Conference and Exhibit*, Salt Lake City, Utah, July 2001.

[3]Oefelein, J. and Yang, V., "Comprehensive Review of Liquid-Propellant Combustion Instabilities in F-1 Engines," *Journal of Propulsion and Power*, Vol. 9, No. 5, September-October 1993, pp. 657–677.

[4]Harvazinski, M., Huang, C., Sankaran, V., Feldman, T., Anderson, W., Merkle, C., and Talley, D., "Instability Mechanism in a Pressure-coupled Gas-gas coaxial rocket injector," *49th AIAA/ASME/SAE/ASEE Joint Propulsion Conference and Exhibit*, AIAA, San Jose, CA, July 2013.

[5]Garby, R., Selle, L., and Poinsot, T., "Analysis of the impact of heat losses on an unstable model rocket-engine combustor using large-eddy simulation," AIAA, Atlanta, GA, July 2012, AIAA Paper 2012-4085.

[6]Garby, R., Selle, L., and Poinsot, T., "Large-Eddy Simulation of Combustion Instabilities in a Variable-length Combustor," *Comptes Rendus Mécanique*, Vol. 341, No. 1-2, 2013, pp. 220–229.

[7]Harvazinski, M., Anderson, W., and Merkle, C., "Analysis of Self-Excited Combustion Instability using Two- and Three-Dimensional Simulations," *Journal of Propulsion and Power*, Vol. 29, No. 2, 2013, pp. 396–409.

[8]Angelberger, C., Veynante, D., and Egolfopoulos, F., "LES of Chemical and Acoustic Forcing of a Premixed Dump Combustor," *Flow, Turbulence and Combustion*, Vol. 65, 2000, pp. 205–222.

[9]Schmitt, P., Poinsot, T., Schuermans, B., and Geigle, K., "Large-eddy simulation and experimental study of heat transfer, nitric acid and combustion instability in a swirled high-pressure burner," *Journal of Fluid Mechanics*, Vol. 570, 2007, pp. 17–46.

[10]Huang, Y., Sung, H., Hsieh, S., and Yang, V., "Large-Eddy Simulation of Combustion Dynamics of Lean-Premixed Swirl-Stabilized Combustor," *Journal of Propulsion and Power*, Vol. 19, No. 5, September-October 2003, pp. 782–794.

[11]Wolf, P., Gicquel, L., Staffelbach, G., and Poinsot, T., "Grid Effects on LES Thermo-Acoustic Limit-Cycle of a Full Annular Aeronautical Engine," *Quality and Reliability of Large-Eddy Simulations II*, Vol. 16 of *ERCOFTAC Series*, Springer Netherlands, 2011, pp. 231–240.

[12]Kaufmann, A., Nicoud, F., and Poinsot, T., "Flow Forcing Techniques for Numerical Simulation of Combustion Instability," *Combustion and Flame*, Vol. 131, No. 4, December 2002, pp. 371–385.

[13]Martin, C., Benoit, L., Sommerer, Y., Nicoud, F., and Poinsot, T., "Large-Eddy Simulation and Acoustic Analysis of a Swirled Staged Turbulent Combustor," *AIAA Journal*, Vol. 44, No. 4, April 2006, pp. 741–750.

[14]Yu, Y., Sisco, J., Rosen, S., Madhav, A., and Anderson, W., "Spontaneous Longitudinal Combustion Instability in a Continuously-Variable Resonance Combustor," *Journal of Propulsion and Power*, Vol. 28, No. 5, 2012, pp. 876–887.

[15]Harvazinski, M., Sankaran, V., and Talley, D., "Parametric Trends in the Combustion Stability Characteristics of a Single-Element Gas-Gas Rocket Engine," *52nd Aerospace Sciences Meeting*, AIAA, National Harbor, MD, January 2014.

[16]Lilley, D., "Swirl Flows in Combustion: A Review," *AIAA Journal*, Vol. 15, No. 8, 1977, pp. 1063–1078.

[17]Huang, Y. and Yang, V., "Dynamics and stability of lean-premixed swirl-stabilized combustion," *Progress in Energy and Combustion Science*, Vol. 35, 2009, pp. 293–364.

[18]Bazarov, V., Yang, V., and Puri, P., "Design and Dynamics of Jet and Swirl Injectors," *Liquid Rocket Thrust Chambers: Aspects of Modeling, Analysis, and Design*, edited by V. Yang, M. Habiballah, J. Hulka, and M. Popp, AIAA, Reston, VA, 2004, pp. 19–103.

[19]Feldman, T., Harvazinski, M., Merkle, C., and Anderson, W., "Comparison Between Simulation and Measurement of Self-Excited Combustion Instability," *48th AIAA/ASME/SAE/ASEE Joint Propulsion Conference and Exhibit*, AIAA, Atlanta, GA, July 2012.

[20]Li, D., Xia, G., Sankaran, V., and Merkle, C., "Computational Framework for Complex Fluids Applications," *3rd International Conference on Computational Fluid Dynamics*.

[21]Lian, C., Xia, G., and Merkle, C., "Solution-Limited Time Stepping to Enhance Reliability in CFD Applications," *Journal of Computational Physics*, Vol. 228, 2009, pp. 4836–4857.

[22]Lian, C., Xia, G., and Merkle, C., "Impact of Source Terms on Reliability of CFD Algorithms," *Computers and Fluids*, 2010.

[23]Westbrook, C. and Dryer, F., "Simplified Reaction Mechanisms for the Oxidation of Hydrocarbon Fuels in Flames," *Combustion Science and Technology*, Vol. 27, 1981, pp. 31–43.

[24]Spalart, P., Jou, W., Strelets, M., and Allmaras, S., "Comments on the feasibility of LES for wings on a hybrid RANS-LES approach," *1st U.S. Air Force Office of Scientific Research Office Conference on DNS/LES*, Columbus, OH, August 1997, pp. 137–148.

[25]Travin, A., Shur, M., and Splart, P., "Physical and numerical upgrades in the detached-eddy simulation of complex turbulent flows," *412 EUROMECH Colloquium on LES of Complex Transitional and Turbulence Flows*, Munich, October 2000.

[26]Wilcox, D., "Formulation of the k-ω turbulence model revisited," *45th AIAA Aerospace Sciences Meeting and Exhibit*, AIAA, Reno, NV, January 2007.

[27]Sisco, J., *Measurement and Analysis of Unstable Model Rocket Combustor*, Ph.D. thesis, Purdue University, West Lafayette, IN, August 2007.

[28]Harvazinski, M., *Modeling Self-Excited Combustion Instabilities Using a Combination of Two- and Three-Dimensional Simulations*, Dissertation, Purdue University, West Lafayette, May 2012.